

A Smart Sensing Grid for Road Traffic Detection Using Terrestrial Optical Networks and Attention-Enhanced Bi-LSTM

*Original*

A Smart Sensing Grid for Road Traffic Detection Using Terrestrial Optical Networks and Attention-Enhanced Bi-LSTM / Usmani, Fehmida; D'Amico, Andrea; Straullu, Stefano; Aquilino, Francesco; Bratovich, Rudi; Virgillito, Emanuele; Curri, Vittorio. - In: JOURNAL OF LIGHTWAVE TECHNOLOGY. - ISSN 0733-8724. - (2025), pp. 1-12.  
[10.1109/jlt.2025.3543180]

*Availability:*

This version is available at: 11583/2998464 since: 2025-03-20T23:37:10Z

*Publisher:*

IEEE

*Published*

DOI:10.1109/jlt.2025.3543180

*Terms of use:*

This article is made available under terms and conditions as specified in the corresponding bibliographic description in the repository

*Publisher copyright*

IEEE postprint/Author's Accepted Manuscript

©2025 IEEE. Personal use of this material is permitted. Permission from IEEE must be obtained for all other uses, in any current or future media, including reprinting/republishing this material for advertising or promotional purposes, creating new collecting works, for resale or lists, or reuse of any copyrighted component of this work in other works.

(Article begins on next page)

# A Smart Sensing Grid for Road Traffic Detection Using Terrestrial Optical Networks and Attention-Enhanced Bi-LSTM

Fehmida Usmani<sup>1</sup>, Andrea D'Amico<sup>2</sup>, Stefano Straullu<sup>3</sup>, Francesco Aquilino<sup>3</sup>, Rudi Bratovich<sup>4</sup>, Emanuele Virgillito<sup>5</sup>, and Vittorio Curri<sup>5</sup>

<sup>1</sup>National University of Computer & Emerging Sciences, Pakistan

<sup>2</sup>NEC Laboratories America, Inc., USA

<sup>3</sup>Links Foundation, Italy

<sup>4</sup>SMOptics, Italy

<sup>5</sup>Politecnico di Torino, Italy

**Abstract**—We demonstrate the use of existing terrestrial optical networks as a smart sensing grid, employing a bidirectional long short-term memory (Bi-LSTM) model enhanced with an attention mechanism to detect road vehicles. The main idea of our approach is to deploy a fast, accurate and reliable trained deep learning model in each network element that is constantly monitoring the state of polarization (SOP) of data signals traveling through the optical line system (OLS). Consequently, this deployment approach enables the creation of a sensing smart grid that can continuously monitor wide areas and respond with notifications/alerts for road traffic situations. The model is trained on the synthetic dataset and tested on the real dataset obtained from the deployed metropolitan fiber cable in the city of Turin. Our model is able to achieve 99% accuracy for both synthetic and real datasets.

**Index Terms**—Fiber optic sensing, machine learning, road traffic detection, smart sensing grid.

## I. INTRODUCTION

**R**OAD transportation plays a vital role in modern cities and civilizations, yet it extracts a heavy toll, with 20–50 million injuries and 1.19 million fatalities happening each year globally [1]. Therefore, it becomes essential to keep up constant traffic monitoring to maintain continuous traffic flow. Essential information on traffic jams and accidents is provided by real-time road traffic monitoring. Using this data, traffic control centers are better equipped to react to accidents quickly and apply intelligent transportation system solutions, such as lane closures or the temporary use of hard shoulders, when needed. Real-time traffic management and intelligent road pavement are two recent developments in the field of smart infrastructure [2]–[4]. Real-time traffic flow is continuously monitored and controlled, which helps to identify unusual behavioural patterns and adjust traffic signal management and regulation to reduce traffic congestion.

Various technologies are presently employed in traffic monitoring systems, relying on sensors placed above, below, or next to highways to measure traffic volume. A variety of technologies are covered by these sensors, such as video cameras [5], infrared [6], radar [7], ultrasonic [8], acoustic [9], and magnetic [10]. Vehicle flow is measured by

processing changes in the magnetic field brought about by passing vehicles. Nevertheless, these techniques are costly and challenging to install and manage. Moreover, they are vulnerable to damage and environmental interference. Solutions that are stable, economical, reliable, precise, and durable are crucial to overcoming the aforementioned challenges in traffic monitoring.

Recently, Optical fibre became an excellent candidate for environmental monitoring with sensing technology since it has remarkable intrinsic qualities in addition to its ability for high-speed data transfer [11]. To enable sensing over wide areas, fibre optic sensing (FOS) makes use of the already deployed telecommunication fibre infrastructure [12]. Over the past few decades, the topic of FOS has drawn a lot of interest from the research community and engineers across different fields [13], [14]. FOSs are outperforming traditional electrical sensors because of their popularity for precision, robustness, tolerance to electromagnetic interference, and comparatively cheap power consumption and lifetime costs [15]. Utilizing the physical characteristics of light waves and their interaction with the surroundings has facilitated the development of FOS designs capable of sensing pressure, humidity, viscosity, acceleration, rotation, magnetic fields, temperature, acoustic signals, and acceleration. FoS finds its applications in various fields including oil and gas [16], aerospace [17], civil engineering [18], biomedical [19], energy [20], and transportation [21].

The core idea of most FOS methods revolves around the measurement of changes in the frequency, intensity, phase, and state of polarization (SOP) of light waves. It is important to note that, even though many FOS applications rely on specialised hardware like distributed acoustic sensors (DAS), phase-sensitive optical time-domain reflectometers (OTDRs), or interferometric setups, these methods have demonstrated excellent performance in terms of event detection and localization. However, the deployment and maintenance of OTDR and DAS-based solutions are costly, especially for large-scale networks or deployments spanning wide areas. This includes the cost of installation, calibration, specialized hardware, and continuous maintenance. Furthermore, because the optical

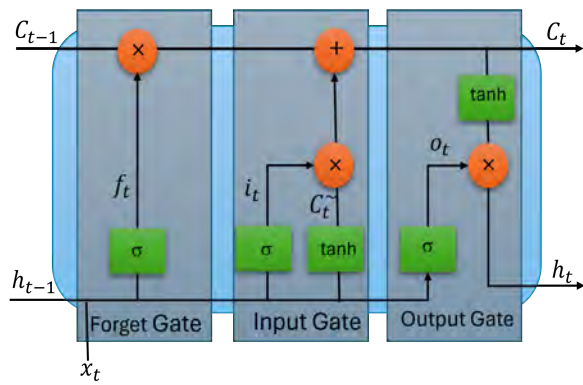


Fig. 1. An LSTM cell

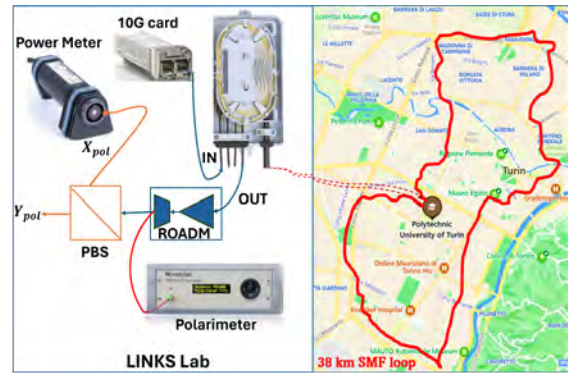


Fig. 2. Experimental setup

isolators within the amplifiers prevent the backscattered DAS signals, these sensing approaches are incompatible with inline optical amplifiers, which frequently exist within the optical fibers. Meanwhile, interferometric methods demand expensive devices. Another viable approach is to compute the SOP fluctuations using the optical lines that have already been implemented instead of utilizing specialized equipment [22]. [23] discussed SOP-based strategy in detail for applications like underwater seismic detection. Furthermore, work in [24]–[27] demonstrates the potential of SOP-based sensing for automatic network downtime detection, network-wide health monitoring, cable break monitoring, and seismic sensing.

In this study, our proposed approach aims to utilize the entire terrestrial optical network as an integrated smart sensing grid. The objective is to detect road traffic and generate notifications without the need for costly additional equipment and eliminate the necessity for dedicated dark fibers. This is enabled by a smart sensing grid optical network’s centralized architecture. Utilizing the existing telecommunications infrastructure allows for the accessibility of several sensing sources across wide terrestrial regions. In this context, we monitor changes in the SOP in coherent channels [23] or intensity-modulated optical channels [22] resulting from mechanical stress induced by passing vehicles. Specifically, since service channels are received at each amplification site, they can offer a wide range of sensing sources. While numerous studies have explored phase and polarization monitoring, one important point remains unanswered: regardless of the measured parameter, how can specific events, such as traffic be detected on incoming waveforms.

Deep learning (DL) based approaches emerged as a promising solution to accomplish this task, as they enable the segmentation or identification of events based on an understanding of the key characteristics that distinguish them. These approaches have substantially enhanced the sensing capabilities of FOS [28]–[30]. The detection and categorization of harmful fiber events [31], anomaly detection in optical networks [32], and earthquake detection [33] are some examples of works that highlight the benefits of using DL in FOS. Since DL techniques have contributed to substantial advancements in applications for traffic monitoring, detecting road traffic in SOP observations has not received much attention, especially

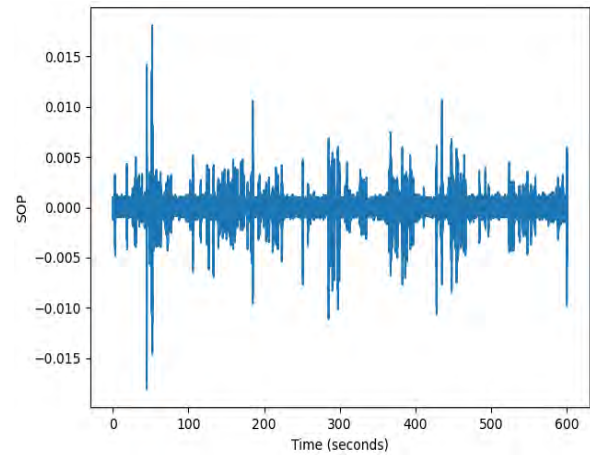


Fig. 3. Real dataset SOP measurements

for one based on a real SOP dataset obtained from an experimental setting. In our previous work [34], we investigate an unsupervised autoencoder-based long short-term memory (LSTM) model for detecting road traffic patterns on real-time SOP measurements of 96 hours. In [35], [36], we develop an early warning earthquake smart sensing system based on SOP measurements and demonstrate its effectiveness in realistic scenarios.

In this work, we present a low-cost hardware-based smart sensing grid architecture that utilizes 10G transceivers and polarization beam splitters (PBS) to observe SOP variations. The DL model based on a bidirectional long short-term memory (Bi-LSTM) with an attention mechanism is integrated into each network element (NE) of existing terrestrial optical networks. This integration allows for effective monitoring and detection of road vehicles, leveraging the low-cost hardware to gather SOP data, which is then processed by the DL model embedded in the network elements. Our objective is to enhance environmental sensing services, particularly for road traffic detection. The PBS monitors state of polarization (SOP) variations in data signals transmitted through the optical line system (OLS). These SOP variations are then analyzed by the DL model, which is implemented in each NE. Importantly, our approach utilizes the existing infrastructure primarily designed for data communication, repurposing it seamlessly for sensing

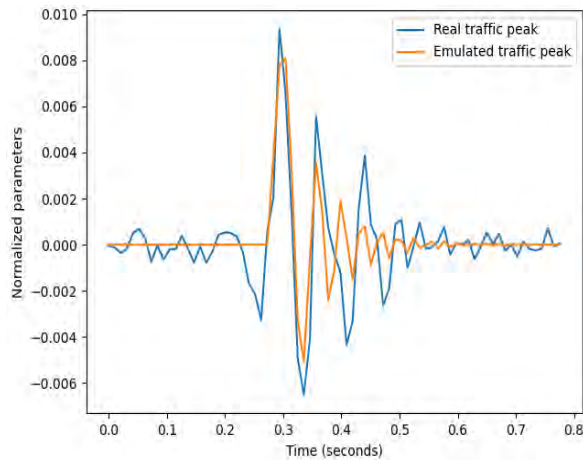


Fig. 4. SOP footprint of vehicle passage

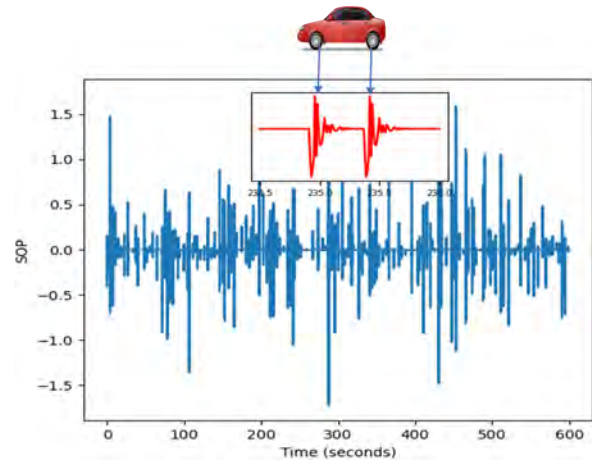


Fig. 5. SOP measurements and vehicle passage event

without requiring any dedicated costly hardware. This dual-use strategy optimizes resource utilization while ensuring fast, accurate, and robust detection of road traffic patterns. By leveraging PBS for SOP detection and the DL model for data analysis within the network elements, our architecture enables the development of a smart sensing grid capable of continuous and precise monitoring over large areas.

The main contributions of our work include the following:-

- We propose to integrate a Bi-LSTM with an attention mechanism model on every NE in the smart sensing grid, which processes the sequences in forward and backward directions simultaneously with an attention mechanism to detect vehicle passing events in an optical fiber sensing network.
- Due to the scarcity of labeled real data, we generated a synthetic labeled dataset mimicking the real dataset to train our proposed supervised learning model.
- The real dataset acquired from the deployed metropolitan fiber cable in the city of Turin is used to evaluate the performance of our proposed model. The obtained results demonstrate that our approach achieves notable accuracy, precision, recall, and F1-score, indicating its effectiveness in road traffic detection.

The rest of the paper is structured as follows:- Section II details our proposed methodology's background knowledge. Section III discusses the dataset generation procedure for real and synthetic datasets and data pre-processing steps. A thorough explanation of our proposed methodology is given in Section IV. The performance analysis of our proposed approach is provided in Section V. Finally, the conclusion and the future directions are given in Section VI.

## II. BACKGROUND ON PROPOSED METHODOLOGY

This section provides details about the two primary components of our proposed DL model.

### A. Long Short Term Memory (LSTM)

The basic building block of our proposed approach is a long short-term memory (LSTM) cell. LSTM is an enhanced version of recurrent neural networks (RNN), it addresses the key

challenge of vanishing gradient problem faced by traditional RNNs. The vanishing gradient problem occurs when network learning is impeded by a large decrease in the gradients of the network weights during back-propagation. LSTM networks overcome this challenge with the use of specific gates that regulate information flow inside the network. These gates allow information to be selectively retained or excluded across longer sequences, which promotes efficient learning over longer times. Long-term dependencies in sequential data are also well-captured by LSTM networks, which increases their usefulness in a variety of applications [37]. The components of a typical LSTM unit are shown in Fig 1, which consists of a cell comprising input, output, and forget gates. These gates control the information that enters and leaves the cell, and the cell stores data for varying durations of time. The forget gate, input gate, and output gate are the three fundamental gates of the LSTM unit, and examining their functions can lead to a thorough grasp of how the unit operates.

- **Forget Gate:** The forget gate's main objective is to assess whether bits within the cell state are relevant. The neural network uses input from both the current input data and the past hidden state to accomplish this task. The network creates a vector with a sigmoid activation function in which each element ranges between 0 and 1. The output from the forget gate is given in Equation 1.

$$f_t = \sigma(W_f \cdot [h_{t-1}, x_t] + b_f), \quad (1)$$

where  $f_t$  represents the forget gate activation vector at the time step  $t$ .  $\sigma$  denotes the sigmoid activation function.  $W_f$  is the weight matrix specific to the forget gate.  $h_{t-1}$  signifies the previous hidden state.  $x_t$  represents the current input at the time step  $t$ .  $b_f$  is the bias vector for the forget gate.

- **Input Gate:** The input gate of an LSTM decides which data should be stored in the cell state  $C_t$  from the current input and the previous hidden state. It is composed of a bias term and a weighted sum of the concatenated input, applied with a sigmoid activation function as illustrated in Equation 2.

$$i_t = \sigma(W_i \cdot [h_{t-1}, x_t] + b_i), \quad (2)$$

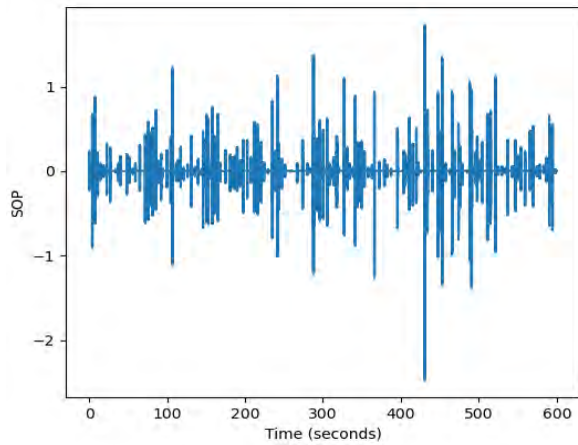


Fig. 6. Variation in time of the SOP vector  $S_1$  component.

where  $i_t$  represents the input gate vector at the time step  $t$ .  $W_i$  is the weight matrix for the input gate.  $h_{t-1}$  is the previous hidden state.  $x_t$  is the current input.  $b_i$  is the bias vector for the input gate. Following the computation of the input gate vector  $i_t$ , the cell state  $C_t$  is updated by the input gate. Equation 3 updates the cell state:

$$C_t = f_t \odot C_{t-1} + i_t \odot \tilde{C}_t \quad (3)$$

where  $\odot$  represents element-wise multiplication,  $\tilde{C}_t$  is the candidate cell state, which contains new information from the current input and the previous hidden state.  $C_{t-1}$  is the previous cell state. The forget gate  $f_t$  controls how much of the previous cell state  $C_{t-1}$  should be retained, while the input gate  $i_t$  determines how much of the candidate cell state  $\tilde{C}_t$  should be incorporated into the updated cell state  $C_t$ . This mechanism effectively allows the model to balance retaining past information and incorporating relevant new information.

- **Output Gate:** The main purpose of the output gate of the LSTM's network is to determine which portions of the cell state are appropriate to be shown as the LSTM cell's output. To create the output, it integrates data from the previous cell state, the prior hidden state, and the current input. Equation 4 shows the output that an output gate produces.

$$o_t = \sigma(W_o \cdot [h_{t-1}, x_t] + b_o), \quad (4)$$

where  $o_t$  is the output gate vector at the time step  $t$ .  $\sigma$  is the sigmoid activation function.  $W_o$  is the weight matrix for the output gate.  $h_{t-1}$  is the previous hidden state.  $x_t$  is the current input.  $b_o$  is the bias vector for the output gate.

### B. Bidirectional LSTM

An LSTM layer comprises several LSTM cells that process input data only in the forward direction. Conversely, a Bidirectional LSTM (Bi-LSTM) adds another LSTM layer that operates in a backward direction. Training two separate unidirectional LSTM networks is similar to training a Bi-LSTM network. One network learns from the original input

sequence, while the other learns from a reversed version of the input sequence. By providing the network with greater contextual knowledge, this approach enables the network to understand the problem more quickly and thoroughly.

### C. Attention Mechanism

The attention mechanism plays a key role in many contemporary neural network architectures, especially for sequence-based tasks [38]. It allows the model to prioritize distinct portions of the input sequence by focusing on particular segments of the sequence. Basically, for every element in the input sequence, the attention mechanism computes a set of attention weights. These weights indicate each element's importance or relevance to the processing step that is currently being performed. By doing this, the model is able to dynamically change its focus during the sequence, giving more weight to important parts and less weight to irrelevant ones. Usually, representations of each element in the sequence are compared with the model's current state to determine attention weights. A compatibility function is frequently used for this comparison, and then a normalization step is added to ensure that the attention weights add up to one. After the attention weights are calculated, they are applied to the input elements to create a weighted sum, with the weights acting as coefficients. The most important data from the input sequence is summarized in this weighted sum, also known as the context vector, for the current processing stage.

## III. DATASET GENERATION AND PREPROCESSING

In this section, we provide the details of the experimental setup used to acquire a real traffic dataset from the deployed fiber in the city of Turin and thoroughly explain the procedure for synthetic dataset generation and data pre-processing.

### A. Experimental setup

An experimental setup to obtain real traffic data is shown in Fig 2. The setup includes a commercial wavelength division multiplexing (WDM) card with an enhanced small form-factor pluggable (SFP+) transceiver (TRX) module acting as the optical source at the transmitter side. This optical signal passes through a 38 km fiber installed across Turin, with its intensity modified at 10 Gbps to carry data. The signal is received by a commercial re-configurable add/drop multiplexer (ROADM) that has a dense WDM filter and inbuilt erbium-doped fiber amplifier. It is accessible from both ends through an optical terminal box at the LINKS laboratory [22]. The ROADM serves as both a 10G dropping node and a pre-amplifier. The detection of polarization change was investigated with two different receiver configurations. The SOP development is monitored with a commercial polarimeter (Novoptel PM-1000) as a baseline. The second setup uses a cascade of polarization beam splitter (PBS) and an optical power meter (OPM) to track power fluctuations of a single polarization state across time. Both techniques are configured to record measurements for up to 96 hours at a sampling rate of 95 samples per second. Both setups are evaluated in [22], where

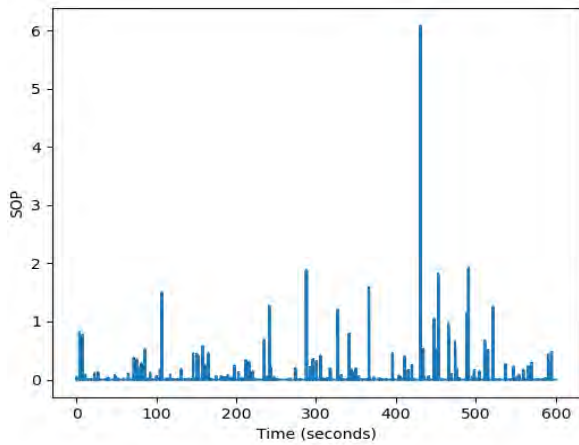


Fig. 7. Time variation square magnitude of the SOP vector.

they show similar dataset characteristics. For this particular work, we acquired the dataset from PBS setup to train our model. Fig. 3 shows the SOP measurements collected for 10-minutes from the experimental setup.

### B. Synthetic dataset generation

In this study, we faced the challenge of an unlabeled SOP dataset acquired from the experimental setup of fiber optic sensing of vehicle passage. The lack of SOP labels makes it challenging to effectively train our supervised learning model. Given the limited number of manually SOP-labeled datasets available, we devised a novel approach to address this issue. Firstly, we extract the pattern by analyzing vehicle-passing events from our experimental setup, capturing the SOP variations induced by different vehicle lengths, speeds, and distances from the fiber-optic sensing system. Using these patterns, we developed a parametric function designed to replicate the observed SOP variations and create synthetic datasets that imitate the event of vehicle passage/no vehicle passage observed in the real data and label them accordingly. The function used to generate a synthetic dataset is expressed as follows:

$$\text{func}(t, t_0, A, \theta, \lambda) = A \sin(\theta s_1^{3/2}) e^{-\lambda s_1} \quad (5)$$

where:

- $t$  is the time variable.
- $t_0$  is the time offset, marking the beginning of the vehicle passage event.
- $A$  is the amplitude parameter, which regulates the SOP signal's strength or magnitude.
- $\theta$  is the shape modulation parameter, which affects how the signal oscillates.
- $\lambda$  is the decay rate parameter that controls how quickly the signal deteriorates over time.
- $s_1 = \text{Heaviside}(t - t_0)$  represents the shifted step function, which guarantees that the signal begins at  $t_0$  and stays constant for  $t < t_0$ .

The synthetic signal is returned by the function `func`, and it consists of the following elements:

- $\sin(\theta \cdot s_1^{3/2})$ : This term causes the signal to exhibit oscillatory behavior, the shape of which is determined by the parameter  $\theta$ .
- $e^{-\lambda \cdot (t-t_0)}$ : The signal is subjected to an exponential decay in this term, with the parameter controlling the rate of decay  $\lambda$ .

By adjusting the values of  $t_0$ ,  $A$ ,  $\theta$ , and  $\lambda$ , synthetic SOP signals generated by the function `func` closely mimic real vehicle passage events observed in the real data. Curve fitting is employed to optimize the parameters  $t_0$ ,  $A$ ,  $\theta$ , and  $\lambda$  of the `func` function. The real and emulated traffic peak is shown in Fig. 4. An 8-hour synthetic dataset is generated by using the optimized parameters  $t_0$ ,  $A$ ,  $\theta$ , and  $\lambda$ . In this process, a variety of variables are arbitrarily selected within predetermined limits, including the length, speed, and distance of vehicles traveling through a fiber-optic sensing system:

- The vehicle length is randomly chosen between 1 and 5 meters.
- The velocity of the vehicles is randomly chosen between 20 and 50 km/h.
- The distance between subsequent vehicles is randomly selected in the range of 20 and 50 meters.

The synthetic dataset is generated by iterating over the specified duration of 10 minutes at a rate of 100 samples per second, resulting in a time difference of 0.01 seconds between each sample. For each iteration, a random number of vehicles is selected within the range of 100 to 200 vehicles, and the time pairs for the front and rear wheels of each vehicle are calculated based on the chosen parameters. These time pairs are then used to label the time axis, indicating the presence of each vehicle in the dataset. The signal is generated for each vehicle. Based on the distributions derived from the optimized parameters, random variations are introduced in the amplitude, shape modulation, and decay rate. The total synthetic dataset is then created by combining the signals produced for every vehicle. The resulting synthetic dataset contains the time axis, combined SOP signal, and corresponding labels. The synthetic dataset for 10-minute SOP signal measurements is demonstrated in Fig. 5. The insights show the waveform (red line) generated during the vehicle passage event.

### C. Data pre-processing

Preprocessing is an essential step in data analysis that aims to improve the quality of data by capturing important characteristics for further analysis tasks. In our proposed approach, we employed two primary pre-processing steps: computing the time variation of the SOP vector,  $\vec{S} = (S_1, S_2, S_3)$ , and then calculating its square magnitude.

- SOP variation: The time variation represents the rate of change of the SOP values. We can identify significant temporal dynamics or trends in the signal by computing the time derivative, which allows us to record fluctuations in the SOP over time. When fast polarization state changes or transitions occur, this step is beneficial in identifying important events or phenomena that could be related to the underlying system. Given the SOP signal

$\vec{S}(t)$ , where  $t$  represents time, the discrete derivative of the SOP for time  $t$  is expressed as follows:

$$\frac{d\vec{S}(t)}{dt} = \left( \frac{dS_1(t)}{dt}, \frac{dS_2(t)}{dt}, \frac{dS_3(t)}{dt} \right)$$

$$\frac{dS_j(t)}{dt} \approx \frac{S_j(t_{i+1}) - S_j(t_i)}{t_{i+1} - t_i} \forall j \in [1, 2, 3] \quad (6)$$

where  $t_i$  and  $t_{i+1}$  are consecutive time points. The time variation of the  $S_1$  component for 10-minute dataset is shown in Fig 6.

- Time variation square magnitude calculation: Following the computation of the time variation, we further process the data by calculating its square magnitude in order to obtain a scalar metric quantifying the SOP variation in time. This emphasizes the magnitude of changes in the SOP while disregarding their direction. This simplification enables robust feature extraction and analysis which helps to concentrate on the whole intensity of fluctuations in the SOP. The time variation square magnitude is expressed as follows:

$$\left| \frac{d\vec{S}(t)}{dt} \right|^2 = \sum_{j=1}^3 \left( \frac{dS_j(t)}{dt} \right)^2 \quad (7)$$

The time variation square magnitude of 10 minute for the SOP measurements is shown in the Fig. 7.

#### IV. BI-LSTM BASED SMART SENSING GRID APPROACH WITH AN ATTENTION MECHANISM FOR AUTOMATIC TRAFFIC DETECTION

##### A. Smart sensing grid approach

Optical networks are turning into dynamically reconfigurable, autonomous systems to handle the complexity brought on by quickly shifting traffic patterns. A centralized optical network controller (ONC), in charge of these systems, interacts with NEs via application programming interfaces (APIs). Using a variety of metrics that are gathered from every NE, the ONC follows the streaming telemetry paradigm to run the network efficiently [39]. Streaming telemetry is a well-known and widely used paradigm in network monitoring and management. The ability to offer real-time visibility into network performance and condition has contributed to its rise in popularity in recent years [40]. Network managers can gather and examine data continuously from different network devices using streaming telemetry, eliminating the need for periodic polling. This framework enables the delivery of diverse services to higher network layers. We propose an extension of the streaming telemetry paradigm to incorporate road traffic detection services seamlessly into the existing network infrastructure, as depicted in Fig. 8. In order to provide network management and control, the streaming telemetry paradigm involves the constant transmission of data from NEs to the ONC. Essential information from devices such as ROADM and amplifiers include power levels and temperature variations, while coherent TRXs capture changes in the phase and SOP of optical signals. Notably, external strain can impact

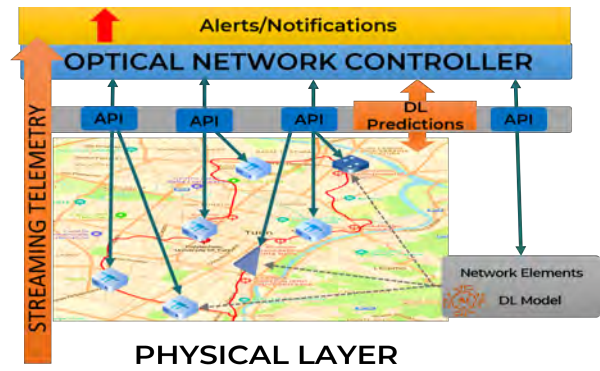


Fig. 8. Architecture of smart sensing network

the phase and SOP of the signal, making SOP changes valuable for sensing purposes as they inherently encode environmental information [41]. Moreover, an integrated post-processing agent in the NEs analyzes, filters, and selectively forwards crucial information to the ONC. In metro and access networks, intensity-modulated direct-detected (IM-DD) TRX remain popular, especially for lower data speeds or functioning as slower optical supervisory channels (OSCs), despite the fact that data from coherent transceivers is frequently inaccessible due to vendor lock-in. OSCs usually come to an end at each amplification site. The polarized nature of IM-DD signals allows for the detection of OSC SOP changes induced by external strains by extracting a small portion of power to supply SOP monitoring devices, such as a simple polarimeter or a PBS [22], [42]. Hence, we propose to integrate the DL model into NEs, offering continuous predictions derived from SOP variations. This utilizes the edge-computing capabilities of NEs, enabling them to transmit timely updates to the ONC, thereby establishing a smart grid network.

##### B. Bi-LSTM with an attention mechanism

This section presents our proposed framework for analyzing the time series data to detect and count road traffic instances using the smart sensing grid approach. Our framework leverages a Bi-LSTM network with an attention mechanism. The suggested model architecture, which has four primary phases, is shown in Figure 9. The algorithm for the proposed approach is illustrated in Algorithm 1. In the following section, we go into detail of each phase.

- Input Data Sequences: The initial phase requires converting the original time-series road traffic dataset into an LSTM cell-compatible format. LSTMs expect input data in the form of 3-dimensional arrays derived from time-series data. The initial dataset is structured into a set of time sequences represented by the notation  $(X_1, X_2, X_3, \dots, X_n)$ . For every sequence  $X$ , there are fixed-length time window data  $(x_1, x_2, x_3, \dots, x_t)$ , where an input of  $m$  features at time instance  $t$  is represented by  $x_t \in \mathbb{R}^m$ . This data is then converted into a two-dimensional array, where the dimensions stand for samples and time steps. For instance, a sequence from our dataset is structured into a 3D array with a shape of

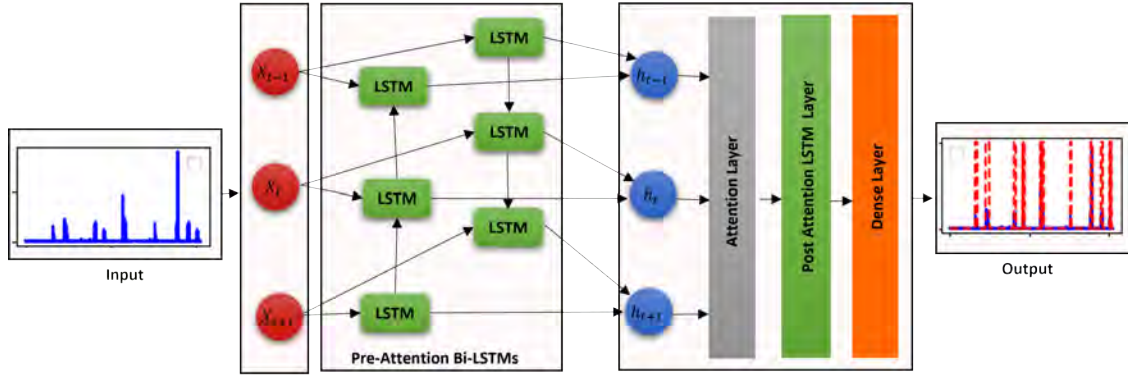


Fig. 9. Architecture of proposed DL model

**Algorithm 1** Traffic Detection Using Bi-LSTM with Attention Mechanism

**Require:**

- 1: Input sequences dataset:  $X$
- 2: Number of sequences:  $N$
- 3: Number of time steps per sequence:  $T_x$
- 4: Number of features per time step:  $m$
- 5: Number of units in Bi-LSTM pre-attention layer:  $n_a$
- 6: Number of units in Bi-LSTM post-attention layer:  $n_s$
- 7: Attention weight matrix:  $W_a$
- 8: Number of training epochs:  $T_{train}$
- 9: Learning rate:  $lr$

**Ensure:** Trained model  $M$  for traffic detection.

**Procedure TrafficDetection**

- 10: **Input:**  $X, N, T_x, m, n_a, n_s, W_a, T_{train}, lr$
- 11: Initialize Bi-LSTM network  $M_{BiLSTM}$  with  $n_a$  and  $n_s$  units.
- 12: Initialize attention mechanism  $M_{Attention}$  with  $W_a$ .
- 13: Initialize output layer  $M_{Output}$ .
- 14: **for**  $epoch = 1$  **to**  $T_{train}$  **do**
- 15:     **for each batch**  $B$  **in**  $X$  **do**
- 16:         Forward pass through  $M_{BiLSTM}$  to compute forward and reverse hidden states.
- 17:         Concatenate forward and reverse hidden states to obtain final hidden state  $h$ .
- 18:         Compute attention weights  $a$  using  $M_{Attention}$ .
- 19:         Compute context vector  $c$  using  $a$  and  $h$ .
- 20:         Forward pass through  $M_{Output}$  to generate predictions.
- 21:         Compute loss and perform backward pass through  $M_{Output}$ .
- 22:         Update parameters of  $M_{Output}$  using gradient descent with learning rate  $lr$ .
- 23:     **end for**
- 24: **end for**
- 25: **return** Trained model  $M$  for traffic detection.

(1223, 150, 1). Here, 1223 represents the total number of sequences, 150 represents the number of time steps, and 1 indicates the single feature (SOP in our case) at each time step. This format ensures that each sequence is structured appropriately for input into an LSTM model, with each dimension representing a specific aspect of the data: samples, time steps, and features.

- Bi-LSTM network: Our model takes an input sequence  $X$  to the Bi-LSTM module that enables it to consider data from both previous and next time steps at the same time. It processes the input sequence in forward and reverse directions to produce hidden state  $H$  and cell state  $C$ . The forward and reverse hidden states are computed as follows:

$$\mathbf{h}_t^{\rightarrow} = \text{LSTM}_f(\mathbf{x}_t, \mathbf{h}_{t-1}^{\rightarrow}, \mathbf{c}_{t-1}^{\rightarrow}), \quad (8)$$

$$\mathbf{h}_t^{\leftarrow} = \text{LSTM}_b(\mathbf{x}_t, \mathbf{h}_{t+1}^{\leftarrow}, \mathbf{c}_{t+1}^{\leftarrow}), \quad (9)$$

where  $\mathbf{h}_t^{\rightarrow}$  (Equation 8) and  $\mathbf{h}_t^{\leftarrow}$  (Equation 9) represent forward and reverse hidden states at time  $t$ ,  $x_t$  denotes input at time  $t$ ,  $\mathbf{c}_t^{\rightarrow}$  and  $\mathbf{c}_t^{\leftarrow}$  are the forward and reverse cell states at time  $t$ ,  $\text{LSTM}_f$  and  $\text{LSTM}_b$  represent the forward and reverse LSTM functions, respectively. The forward and backwards hidden states are concatenated to get the final hidden state  $h$ :

$$\mathbf{h} = [\mathbf{h}_1^{\rightarrow}, \mathbf{h}_2^{\rightarrow}, \dots, \mathbf{h}_T^{\rightarrow}, \mathbf{h}_T^{\leftarrow}, \mathbf{h}_{T-1}^{\leftarrow}, \dots, \mathbf{h}_1^{\leftarrow}]$$

In our proposed model, each direction of the Bi-LSTM layer consists of 64 units with a hyperbolic tangent ( $\tanh$ ) activation function, selected through grid search for hyperparameter tuning to effectively capture contextual information.

- Attention layer: The final hidden state  $h$  is passed to the attention mechanism module which computes the attention weights  $e_t$  at different time steps according to the provided hidden and cell states from the Bi-LSTM module as follows: The output  $h$  from the Bi-LSTM layer is used as an input to the attention layer. The attention layer computes the context vector to learn to focus on the most useful information in the input sequences as follows:

$$a = \text{softmax}(W_a \cdot h) \quad (10)$$



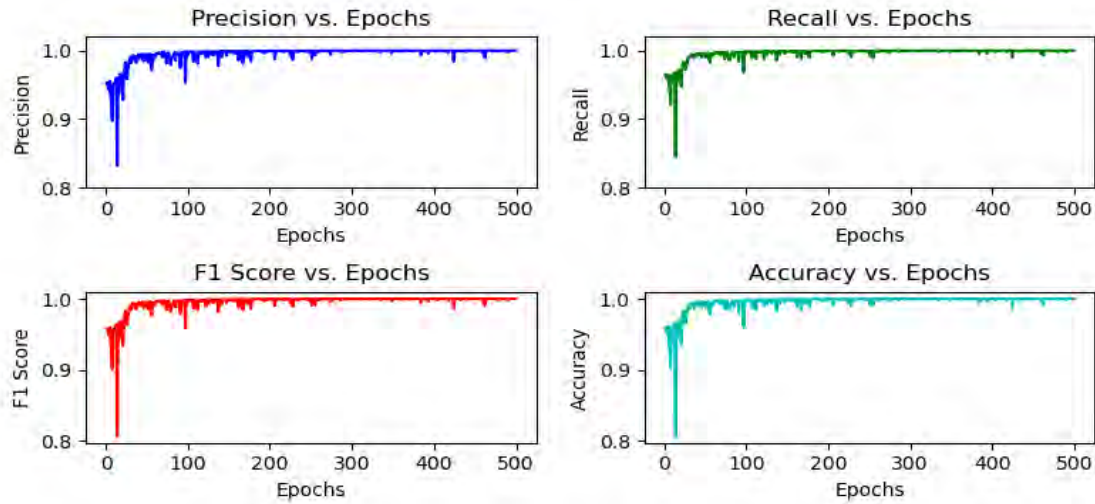


Fig. 10. Precision, Recall, F1 score, and Accuracy on validation dataset

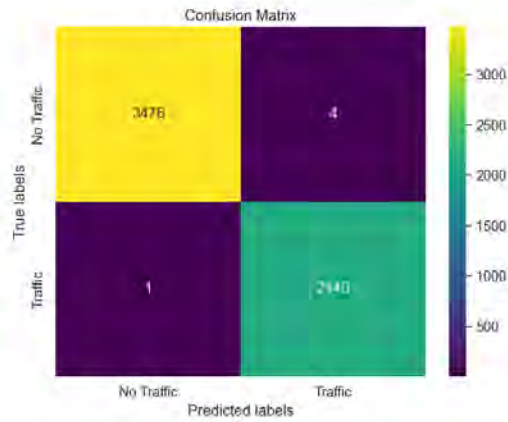


Fig. 11. Confusion matrix.

$$c = \sum_{t=1}^T a_t \cdot h_t \quad (11)$$

where  $W_a$  is the attention weight matrix,  $a$  is the attention weights and  $c$  is the attention context vector.

- **Post-attention LSTM:** The context vectors produced by the attention mechanism are processed by the Post-Attention LSTM Cell in conjunction with its prior hidden and cell states. The post-attention layer in our proposed methods consists of 64 neurons with a  $\tanh$  activation function. The context vectors are weighted according to the attention mechanism's computations and include information about important segments of the input sequence. The attention mechanism provides context, and the LSTM cell, by incorporating the context vectors, is able to grasp dependencies between various time steps in the input sequence. The LSTM cell updates its hidden state and cell state based on the input context vectors and its previous states, enabling it to adjust to the dynamics

of the sequence and develop the ability to produce precise predictions.

- **Traffic detection:** We employ a dense layer with a sigmoid activation function as the output layer in our model, which consists of a single neuron. The output layer uses the post-attention LSTM's hidden state to predict the output at each time step. The knowledge gained from the input sequence and the context given by the attention mechanism are combined in the hidden state of the post-attention LSTM. The output layer generates the output prediction at each time step by applying the sigmoid activation function to the post-attention LSTM's hidden state. Based on the input sequence and the context data obtained from the attention mechanism, the output values represent the model's prediction of the likelihood of traffic being detected.

## V. PERFORMANCE ANALYSIS

In this section, we describe the model training process, the evaluation measures used to assess the model's performance and the results.

### A. Model training and evaluation metrics

The model is trained using an adaptive learning rate optimization (adam) technique. The learning rate for every parameter is modified by taking into account approximations of the gradients' first and second moments. Training is done using the binary cross-entropy loss function, which is specified as follows:

$$\text{Binary Crossentropy}(y_{\text{true}}, y_{\text{pred}}) = -\frac{1}{N} \sum_{i=1}^N \left( y_{\text{true}}^{(i)} \cdot \log(y_{\text{pred}}^{(i)}) + (1 - y_{\text{true}}^{(i)}) \cdot \log(1 - y_{\text{pred}}^{(i)}) \right), \quad (12)$$

where  $y_{\text{true}}$  represents the true labels or ground truth values, while  $y_{\text{pred}}$  represents the predicted probabilities generated

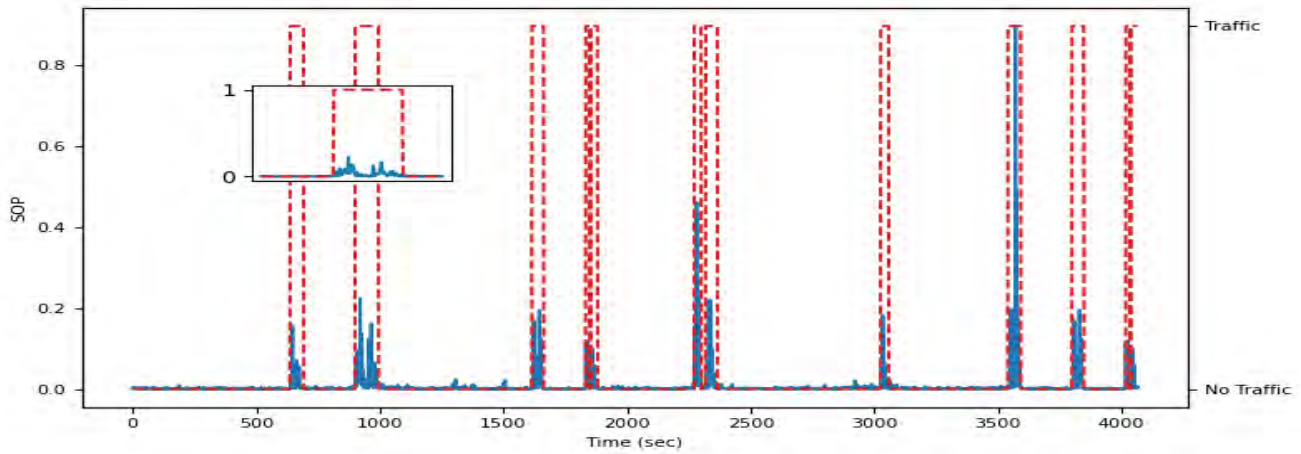


Fig. 12. DL model predictions on real dataset.

by the model.  $N$  denotes the total number of samples.  $y_{\text{true}}^{(i)}$  and  $y_{\text{pred}}^{(i)}$  represent the true label and predicted probability (or score) for the  $i$ -th sample, respectively. The expression  $y_{\text{true}}^{(i)} \cdot \log(y_{\text{pred}}^{(i)})$  calculates the cross-entropy loss for the positive class, while  $(1 - y_{\text{true}}^{(i)}) \cdot \log(1 - y_{\text{pred}}^{(i)})$  calculates the cross-entropy loss for the negative class. The overall loss is the average of these per-sample losses over all  $N$  samples.

The model is trained exclusively on the synthetic dataset, allowing it to learn the intricate relationships between vehicle-induced perturbations and their corresponding SOP variations. To evaluate our model's performance and ensure its applicability to real-world data, we conducted a validation phase using a carefully curated dataset. We extracted specific vehicle passage patterns from our experimental setup and manually labeled a limited set of real-world data. The proposed model is trained using a synthetic time series of 8-hour dataset files that mimic real-world scenarios with a learning rate of 0.0001. Each data file has a single feature, defined as the norm of SOP variation over time. During the training phase, 60% of the dataset is used to train the model, while 20% for validation and another 20% for testing purposes. In terrestrial scenarios, SOP measurements can often be affected by polarization noise originating from various anthropic activities. We added 10% Gaussian noise to the original signal to simulate real-world environmental circumstances and assess the robustness of the model. This noise level is determined by considering the variance of the original signal. During training, the adam optimizer uses the binary cross-entropy loss function to compute gradients to adjust the model parameters. The best weights for the model are restored by early stopping, which is used to monitor the validation loss and terminate training if there is no improvement after 3 epochs. For a total of 500 epochs, the training data is fed into the model in batches of size 16. The grid search method is employed to tune the hyperparameters of the model such as learning rate, batch size, and number of units in the hidden layers.

To assess the performance of our proposed model, we employ accuracy, precision, recall, and F1 score metrics described in Equations 13, 14, 15 and 16 as follows:

$$\text{Accuracy} = \frac{TP + TN}{TP + TN + FP + FN} \quad (13)$$

The overall precision of the model's predictions is measured by accuracy. The number of cases accurately predicted as "traffic detected" is known as true positives (TP). True negatives (TN) represent the number of cases where "traffic not detected" is accurately anticipated. The number of cases that are mistakenly reported as "traffic detected" while none are known as false positives (FP). The number of cases where "traffic not detected" is mistakenly predicted when in fact there is traffic is represented as false negatives (FN).

$$\text{Precision} = \frac{TP}{TP + FP} \quad (14)$$

Precision is used to measure the proportion of true positives among all of the model's positive predictions.

$$\text{Recall} = \frac{TP}{TP + FN} \quad (15)$$

Out of all actual positives, recall quantifies the percentage of true positives that the model properly detected.

$$\text{F1 Score} = 2 \times \frac{\text{Precision} \times \text{Recall}}{\text{Precision} + \text{Recall}} \quad (16)$$

It is difficult to evaluate classification model performance accurately when imbalanced datasets are present. Conventional accuracy measures could have a bias towards the majority class, which could conceal the model's actual effectiveness. Given this, another reliable metric for assessing detection performance is the F1 measure. The F1 score is especially useful for imbalanced datasets because it achieves a balance between precision and recall.

## B. Results

The precision, recall, F1 score, and accuracy of our model are shown in Fig. 10 on the validation dataset during the training process across 500 epochs. The model was trained for 500 epochs, and checkpoints were saved periodically based

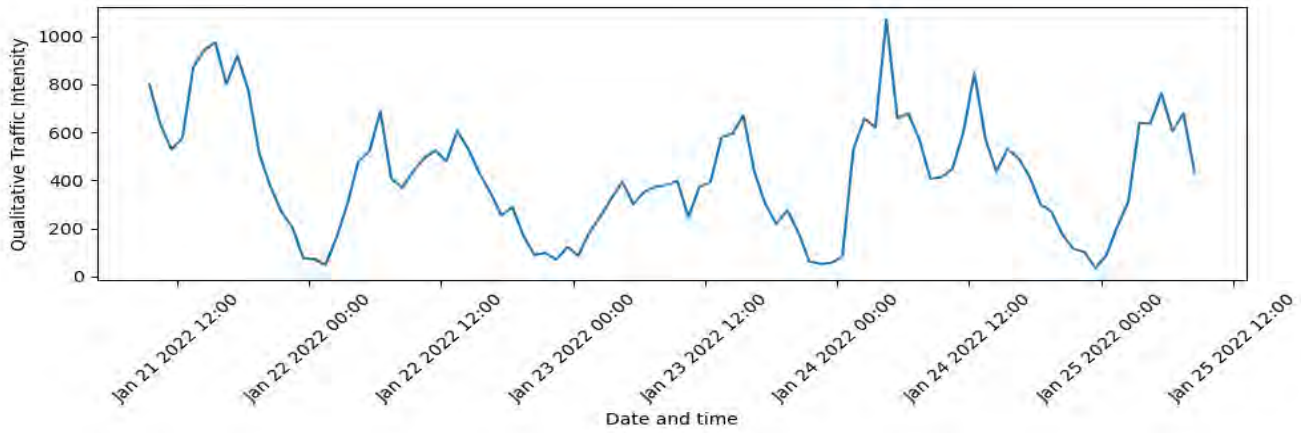


Fig. 13. Relative Traffic Activity

on validation performance. After analyzing the training and validation accuracy trends, it was observed that the validation accuracy stabilized around the 400th epoch with minimal fluctuations and close alignment to the training accuracy. Therefore, the checkpoint corresponding to this range was selected for testing, as it demonstrated the best generalization performance. The results demonstrate that every metric performs consistently and promisingly, with an accuracy rate of around 99%. This indicates that the model is effectively trained and demonstrates strong performance even on unseen data during training. In Fig. 11, we present a confusion matrix to visualize the performance of a model for classifying traffic and no traffic. The findings demonstrate that the model accurately identifies 2140 out of 2141 traffic instances, resulting in an accuracy of 99.9%. Fig. 12 shows the model performance on a few vehicle passage events on a real dataset. Red dashed lines show the model predictions for label 0 (no traffic) and label 1 (traffic). The main goal of our model is to identify the arrival of a leading wheel (wheel 1) and the trailing wheel (wheel 2) of a vehicle. The arrival of wheel 1 is indicated by a signal peak, followed by a subsequent peak of wheel 2. Our model is able to correctly identify the vehicle passage event starting from the arrival of wheel 1 and ending on the passage of wheel 2 as shown in zoomed in part of the Fig. 12. The model is also clearly able to distinguish between the noise and the actual event. In order to further investigate the efficacy of our proposed method, we computed a qualitative representation of traffic activity per hour for the full 96-hour real dataset starting from January 21, 2022, at 09:30 AM, as shown in Fig. 13. The results demonstrate how well our proposed approach captures hourly and daily traffic trends. Notably, there are noticeable variations in patterns from day to night and weekdays to Sundays, which closely correspond with expected traffic trends. It is important to note that the values in Fig. 13 do not represent exact vehicle counts but rather a qualitative traffic intensity based on SOP variations. Additionally, we compared the relative traffic activity detected by our method with the statistics obtained from the experimental setup [22] and our manually labeled dataset from different portions of the 96-hour dataset. The results showed that our method provides

a high correlation with observed traffic trends, indicating its effectiveness in detecting relative changes in traffic activity.

## VI. CONCLUSION AND FUTURE WORK

This study presents a significant advancement in traffic monitoring applications, highlighting the effectiveness of utilizing existing terrestrial optical networks, empowered with deep learning, as a smart sensing grid for road vehicle detection based on SOP measurements. The proposed smart architecture integrates sensing functions into data and service channels with low-cost hardware at the network nodes. Due to the polarized nature of SOP variations, they can be observed on 10G data channels by extracting a portion of the received signal without disrupting data transmission. We monitor the SOP variations by utilizing a 10G commercial transceiver and a polarization beam splitter, ensuring the setup remains simple, cost-effective, and easily integrated into the network nodes. The monitored SOP data is then fed into our proposed deep learning-based model, which detects road vehicles based on SOP variations. Our methodology can reliably detect road vehicles with 99% accuracy, serving as a foundational step in developing an automated traffic monitoring system. This approach offers an intelligent, cost-effective alternative to SOP detection using coherent transceivers and is particularly suitable for metro network segments where 10G channels are still widely utilized. Future work involves incorporating more advanced simulation techniques to explicitly analyze and address the effects of superposition caused by multiple vehicles. This approach provides deeper insights into how SOP variations from different vehicles interact, further enhancing the system's robustness and accuracy in detecting and classifying vehicles in complex traffic scenarios.

## ACKNOWLEDGMENT

Vittorio Curri and Emanuele Virgillito thank the Italian National Recovery and Resilience Plan (NRRP) of NextGenerationEU, partnership on "Telecommunications of the Future" (PE00000001—program "RESTART")

REFERENCES

- [1] G. Cookson, "World Health Organization: Road traffic injuries," [Online], 2023, accessed: 18-Feb-2019. [Online]. Available: <https://www.who.int/news-room/fact-sheets/detail/road-traffic-injuries>
- [2] A. Kutlimuratov, J. Khamzaev, T. Kuchkorov, M. S. Anwar, and A. Choi, "Applying enhanced real-time monitoring and counting method for effective traffic management in tashkent," *Sensors*, vol. 23, no. 11, 2023. [Online]. Available: <https://www.mdpi.com/1424-8220/23/11/5007>
- [3] M. Gupta, H. Miglani, P. Deo, and A. Barhatte, "Real-time traffic control and monitoring," *e-Prime - Advances in Electrical Engineering, Electronics and Energy*, vol. 5, p. 100211, 2023. [Online]. Available: <https://www.sciencedirect.com/science/article/pii/S2772671123001067>
- [4] M. Moradi and G. J. Assaf, "Designing and building an intelligent pavement management system for urban road networks," *Sustainability*, vol. 15, no. 2, 2023. [Online]. Available: <https://www.mdpi.com/2071-1050/15/2/1157>
- [5] K. Robert, "Video-based traffic monitoring at day and night vehicle features detection tracking," in *2009 12th International IEEE Conference on Intelligent Transportation Systems*, 2009, pp. 1–6.
- [6] M. Z. Khalid, A. Tanveer, S. Ahmad, H. Ejaz, and M. H. M. Farrukh, "Optimizing traffic flow: Utilizing ir and load cell sensors for cost-effective traffic congestion alleviation at smart city intersections," *Engineering Proceedings*, vol. 56, no. 1, 2023. [Online]. Available: <https://www.mdpi.com/2673-4591/56/1/43>
- [7] G. Cantisani, G. Del Serrone, R. Mauro, P. Peluso, and A. Pompigna, "Traffic stream analysis by radar sensors on two-lane roads for free-moving and constrained vehicles identification," *Sensors*, vol. 23, no. 15, 2023. [Online]. Available: <https://www.mdpi.com/1424-8220/23/15/6922>
- [8] O. Appiah, E. Quayson, and E. Opoku, "Ultrasonic sensor based traffic information acquisition system; a cheaper alternative for its application in developing countries," *Scientific African*, vol. 9, p. e00487, 2020. [Online]. Available: <https://www.sciencedirect.com/science/article/pii/S2468227620302258>
- [9] G. Szwoch and J. Kotas, "Acoustic detector of road vehicles based on sound intensity," *Sensors*, vol. 21, no. 23, 2021. [Online]. Available: <https://www.mdpi.com/1424-8220/21/23/7781>
- [10] K. Wang, H. Xiong, J. Zhang, H. Chen, D. Dou, and C.-Z. Xu, "Sensemag: Enabling low-cost traffic monitoring using noninvasive magnetic sensing," *IEEE Internet of Things Journal*, vol. 8, no. 22, pp. 16 666–16 679, 2021.
- [11] E. Ip, J. Fang, Y. Li, Q. Wang, M.-F. Huang, M. Salemi, and Y.-K. Huang, "Distributed fiber sensor network using telecom cables as sensing media: technology advancements and applications [invited]," *Journal of Optical Communications and Networking*, vol. 14, no. 1, pp. A61–A68, 2022.
- [12] P. Boffi, "Sensing applications in deployed telecommunication fiber infrastructures," in *2022 European Conference on Optical Communication (ECOC)*, 2022, pp. 1–4.
- [13] A. Mecozzi, C. Antonelli, M. Mazur, N. Fontaine, H. Chen, L. Dallachiesa, and R. Ryf, "Use of optical coherent detection for environmental sensing," *Journal of Lightwave Technology*, vol. 41, no. 11, pp. 3350–3357, 2023.
- [14] M. Mazur, N. Parkin, R. Ryf, A. Iqbal, P. Wright, K. Farrow, N. K. Fontaine, E. Börjeson, K. Kim, L. Dallachiesa, H. Chen, P. Larsson-Edefors, A. Lord, and D. Neilson, "Continuous fiber sensing over field-deployed metro link using real-time coherent transceiver and das," in *2022 European Conference on Optical Communication (ECOC)*, 2022, pp. 1–4.
- [15] C. Pendão and I. Silva, "Optical fiber sensors and sensing networks: Overview of the main principles and applications," *Sensors*, vol. 22, no. 19, 2022. [Online]. Available: <https://www.mdpi.com/1424-8220/22/19/7554>
- [16] I. Ashry, Y. Mao, B. Wang, F. Hveding, A. Y. Bukhamsin, T. K. Ng, and B. S. Ooi, "A review of distributed fiber-optic sensing in the oil and gas industry," *Journal of Lightwave Technology*, vol. 40, no. 5, pp. 1407–1431, 2022.
- [17] A. Rovera, A. Tancau, N. Boetti, M. D. L. Dalla Vedova, P. Maggiore, and D. Janner, "Fiber optic sensors for harsh and high radiation environments in aerospace applications," *Sensors*, vol. 23, no. 5, 2023. [Online]. Available: <https://www.mdpi.com/1424-8220/23/5/2512>
- [18] M. F. Bado and J. R. Casas, "A review of recent distributed optical fiber sensors applications for civil engineering structural health monitoring," *Sensors*, vol. 21, no. 5, 2021. [Online]. Available: <https://www.mdpi.com/1424-8220/21/5/1818>
- [19] D. Tosi and G. Perrone, 2017.
- [20] P. R. Ohodnicki and K. P. Chen, "Optical fiber sensors for energy infrastructure: Emerging opportunities," in *Optical Fiber Sensors Conference 2020 Special Edition*. Optica Publishing Group, 2020, p. T1.1. [Online]. Available: <https://opg.optica.org/abstract.cfm?URI=OFS-2020-T1.1>
- [21] H. Liu, J. Ma, T. Xu, W. Yan, L. Ma, and X. Zhang, "Vehicle detection and classification using distributed fiber optic acoustic sensing," *IEEE Transactions on Vehicular Technology*, vol. 69, no. 2, pp. 1363–1374, 2020.
- [22] R. Bratovich, F. M. R., S. Straullu, E. Virgillito, A. Castoldi, A. D'Amico, F. Aquilino, R. Pastorelli, and V. Curri, "Surveillance of metropolitan anthropic activities by wdm 10g optical data channels," in *2022 European Conference on Optical Communication (ECOC)*, 2022, pp. 1–4.
- [23] A. Mecozzi, M. Cantono, J. C. Castellanos, V. Kamalov, R. R. Muller, and Z. Zhan, "Polarization sensing using submarine optical cables," 2021.
- [24] C. Carver and X. Zhou, "Polarization sensing of network health and seismic activity over a live terrestrial fiber-optic cable," *Communications Engineering*, vol. 3, 07 2024.
- [25] J. C. Castellanos, Z. Zhan, V. Kamalov, M. Cantono, S. Yin, A. Mecozzi, S. Bhattacharya, and R. M. Allen, "Optical polarization-based sensing and localization of submarine earthquakes," in *2022 Optical Fiber Communications Conference and Exhibition (OFC)*, 2022, pp. 1–3.
- [26] M. Cantono, J. C. Castellanos, V. Kamalov, A. Mecozzi, R. Muller, S. Yin, and Z. Zhan, "Seismic sensing in submarine fiber cables," 09 2021, pp. 1–3.
- [27] M. Mazur, D. Wallberg, L. Dallachiesa, E. Börjeson, R. Ryf, M. Bergroth, B. Josefsson, N. K. Fontaine, H. Chen, D. T. Neilson, J. Schröder, P. Larsson-Edefors, and M. Karlsson, "Real-time monitoring of cable break in a live network using a coherent transceiver prototype," in *2024 Optical Fiber Communications Conference and Exhibition (OFC)*, 2024, pp. 1–3.
- [28] A. Venketeswaran, N. Lalam, J. Wuenschell, P. R. Ohodnicki Jr., M. Badar, K. P. Chen, P. Lu, Y. Duan, B. Chorpensing, and M. Buric, "Recent advances in machine learning for fiber optic sensor applications," *Advanced Intelligent Systems*, vol. 4, no. 1, p. 2100067, 2022. [Online]. Available: <https://onlinelibrary.wiley.com/doi/abs/10.1002/aisy.202100067>
- [29] M. Cantono, J. C. Castellanos, S. Batthacharya, S. Yin, Z. Zhan, A. Mecozzi, and V. Kamalov, "Optical network sensing: Opportunities and challenges," in *2022 Optical Fiber Communications Conference and Exhibition (OFC)*, 2022, pp. 1–3.
- [30] A. Rode, M. Farsi, V. Lauinger, M. Karlsson, E. Agrell, L. Schmalen, and C. Häger, "Machine learning opportunities for integrated polarization sensing and communication in optical fibers," *Optical Fiber Technology*, vol. 90, p. 104047, 2025. [Online]. Available: <https://www.sciencedirect.com/science/article/pii/S1068520024003924>
- [31] L. Sadighi, S. Karlsson, C. Natalino, and M. Furdek, "Machine learning-based polarization signature analysis for detection and categorization of eavesdropping and harmful events," 01 2024, p. M1H.1.
- [32] K. Abdelli, M. Lonardi, J. Gripp, D. Correa, S. Olsson, F. Boitier, and P. Layec, "Anomaly detection and localization in optical networks using vision transformer and sop monitoring," in *2024 Optical Fiber Communications Conference and Exhibition (OFC)*, 2024, pp. 1–3.
- [33] F. Usmani, H. Awad, E. Virgillito, R. Bratovich, S. Straullu, F. Aquilino, R. Proietti, R. Pastorelli, and V. Curri, "Earthquake early warning through terrestrial optical networks: A bi-gru attention model approach on sop data," in *Optical Fiber Communication Conference (OFC) 2024*. Optica Publishing Group, 2024, p. Tu3J.2. [Online]. Available: <https://opg.optica.org/abstract.cfm?URI=OFC-2024-Tu3J.2>
- [34] F. Usmani, A. D'Amico, R. Bratovich, M. R. Fransisco, S. Straullu, E. Virgillito, F. Aquilino, R. Pastorelli, and V. Curri, "Road traffic detection with a lstm autoencoder using state of polarization on deployed metropolitan fiber cable," in *2023 International Conference on Optical Network Design and Modeling (ONDM)*, 2023, pp. 1–3.
- [35] F. Usmani, H. Awad, E. Virgillito, R. Bratovich, S. Straullu, F. Aquilino, R. Proietti, R. Pastorelli, and V. Curri, "Earthquake early warning through terrestrial optical networks: A bi-gru attention model approach on sop data," in *Proceedings of Optical Fiber Communications Conference (OFC)*, San Diego, California, United States, 2024, p. Tu3J.2.
- [36] H. Awad, F. Usmani, E. Virgillito, R. Bratovich, R. Proietti, S. Straullu, F. Aquilino, R. Pastorelli, and V. Curri, "Environmental surveillance through machine learning-empowered utilization of optical networks," *Sensors*, vol. 24, no. 10, 2024. [Online]. Available: <https://www.mdpi.com/1424-8220/24/10/3041>

- [37] S. Hochreiter and J. Schmidhuber, "Long Short-Term Memory," *Neural Computation*, vol. 9, no. 8, pp. 1735–1780, 11 1997. [Online]. Available: <https://doi.org/10.1162/neco.1997.9.8.1735>
- [38] G. Brauwers and F. Frasinca, "A general survey on attention mechanisms in deep learning," *IEEE Transactions on Knowledge and Data Engineering*, vol. 35, no. 4, p. 3279–3298, Apr. 2023. [Online]. Available: <http://dx.doi.org/10.1109/TKDE.2021.3126456>
- [39] F. Paolucci, A. Sgambelluri, F. Cugini, and P. Castoldi, "Network telemetry streaming services in sdn-based disaggregated optical networks," *Journal of Lightwave Technology*, vol. 36, no. 15, pp. 3142–3149, 2018.
- [40] J. E. Simsarian, G. Hosangadi, W. Van Raemdonck, J. Gripp, M. N. Hall, J. Yu, and T. Sizer, "Demonstration of cloud-based streaming telemetry processing for optical network monitoring," in *2021 European Conference on Optical Communication (ECOC)*, 2021, pp. 1–4.
- [41] E. Virgillito, S. Straullu, F. Aquilino, R. Bratovich, H. Awad, R. Proietti, A. D'Amico, R. Pastorelli, and V. Curri, "Detection, localization and emulation of environmental activities using sop monitoring of imdd optical data channels," in *2023 23rd International Conference on Transparent Optical Networks (ICTON)*, 2023, pp. 1–4.
- [42] S. Straullu, F. Aquilino, R. Bratovich, F. M. Rodriguez, A. D'Amico, E. Virgillito, R. Pastorelli, and V. Curri, "Real-time detection of anthropic events by 10g channels in metro network segments," in *2022 IEEE Photonics Conference (IPC)*, 2022, pp. 1–2.